



# Mathematical modelling of combined pressure driven and electrokinetic effect in a channel with induced magnetic field: An exact solution

Basant K. Jha, Michael O. Oni\*

Department of Mathematics, Ahmadu Bello University, Zaria, Nigeria

## ARTICLE INFO

### Article history:

Received 16 October 2017

Accepted 16 October 2018

Available online 22 October 2018

### Keywords:

Electrokinetics

Induced magnetic field

Pressure driven

Exact solution

Channel

## ABSTRACT

This article presents exact solution for pressure driven flow formation of electrically conducting fluid in a parallel plate channel formed by two horizontal parallel plates with electrokinetic effects and induced magnetic field. Using the Poisson–Boltzmann, Navier–Stokes equations and induction equation, the governing electric potential, momentum, induced magnetic field and energy equations for the present article are presented and transformed to their corresponding dimensionless form using suitable parameters. The governing dimensionless equations are solved exactly and graphical representation are presented. During the cause of graphical illustration, it is found that the role of electrokinetic effects and Hartmann number is to decrease the electric potential, fluid velocity, induced magnetic field and fluid temperature. A special case is found and discussed when the value of Hartmann number equals the Debye–Hückel parameter. It is interesting to note that heat transfer is independent on governing parameters for large value of Debye–Hückel parameter.

© 2018 The Authors. Production and hosting by Elsevier B.V. on behalf of King Saud University. This is an open access article under the CC BY-NC-ND license (<http://creativecommons.org/licenses/by-nc-nd/4.0/>).

## 1. Introduction

Electrokinetic phenomenon is significant in laboratory, industrial and engineering applications such as the removal of contaminants in soil and imposing electric ion on flow formation. This phenomenon involves the passing of low-voltage direct current electric field across the boundary on a fluid. Other applications can be found in medical field for cardiopulmonary resuscitation and development of battery cells.

When a liquid containing small amount of ions is brought in contact with a solid boundary, the like charges repel while the unlike charges attract. This situation leads to the formation of EDL (electric double layer) closed to the wall containing excess counter ions. Reuss (1809) and Probstein (1994) are the earliest scientists to discover the electrokinetic effects. Reuss (1809) in an experiment on porous clay found that particles dispersed in water migrate due to the constant application of electricity. Later, Helmholtz (1879) developed the EDL theory which relates the elec-

tric and flow parameters for electrokinetics. With increasing interest in understanding electrokinetic flows, many numerical investigations have been carried out. Patankar and Hu (1998) presented numerical simulation of microfluidic injection using electroosmotic forces through intersection of two channels. Ren and Li (Debye and Hückel, 1923) studied electroosmotic flows in microchannels with axially non-uniform zeta potentials and varying cross-sections. Yang and Li (1998) used the Debye–Hückel approximation (Ren and Li, 2001) to develop a numerical algorithm for electrokinetically-driven Newtonian liquid flows. They concluded that for a liquid solution of low ionic concentration and a solid surface of high zeta potential the liquid flow in rectangular microchannels is significantly influenced by the presence of the EDL field and hence deviates from the flow characteristics described by classical fluid mechanics.

Many researches have been committed to study the combined effect of pressure and electrokinetic effects on flow formation in channel (Zade et al., 2007; Mukhopadhyay et al., 2009; Soong and Wang, 2003; Matin and Khan, 2016). Mukhopadhyay et al. (2009) examined the fully developed hydrodynamic and thermal transport in combined pressure and electrokinetically driven flow with asymmetric boundary condition. They established that both flow and heat transfer characteristics are significantly affected by the asymmetries in wall boundary conditions for both purely electroosmotic and combined pressure-driven and electroosmotic flow.

\* Corresponding author.

E-mail address: [michaeloni29@yahoo.com](mailto:michaeloni29@yahoo.com) (M.O. Oni).

Peer review under responsibility of King Saud University.





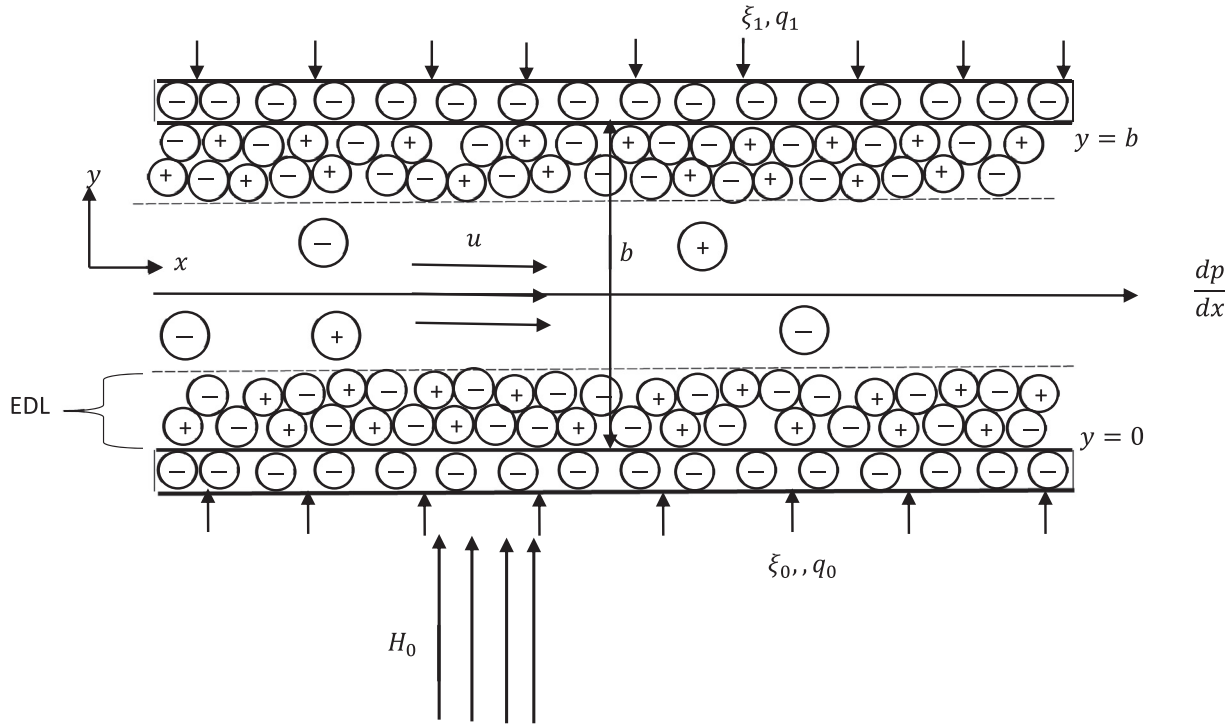


Fig. 1. Schematic of the problem.

- iii. The plates are taken to be either conducting or non-conducting; Case I, both walls are non-conducting, Case II, the wall \$y = 0\$ is conducting while \$y = b\$ is non-conducting, Case III, the wall \$y = 0\$ is non conducting while \$y = b\$ is conducting.
- iv. The walls are negatively charged and the liquid contains an ideal solution of fully dissociated symmetric salt, the EDLs formed on the walls do not overlap, and the temperature variation over the channel cross section is negligible compared with the absolute temperature.
- v. The charge distribution in the EDL follows Boltzmann distribution, hence the ion convection effects are negligible.
- vi. The wall potentials are considered low enough for Debye-Hückel linearization to be valid.
- vii. The external voltage is significantly higher than the flow induced voltage.
- viii. Except otherwise stated, all thermophysical parameters are assumed constant.

2.1. Electric potential distribution

Following above assumptions, the electrical potential distribution is obtained from Poisson-Boltzmann equation (Mukhopadhyay et al., 2009) as:

$$\nabla^2 \phi = \frac{2FzC_0}{\epsilon} \sinh\left(\frac{zF\psi'}{RT}\right) \tag{1}$$

The potential \$\phi\$ is due to combination of externally imposed field and EDL potential \$\psi'\$.

For fully developed flow, the external potential gradient is in the axial direction only, since the wall potentials are assumed low enough for Debye-Hückel linearization to be valid, Eq. (1) in dimensionless form becomes:

$$\frac{d^2 \psi}{dY^2} - \kappa^2 \psi = 0 \tag{2}$$

Subject to

$$\psi(0) = 1, \psi(1) = \xi \tag{3}$$

The details of this derivation can be found in (Mukhopadhyay et al., 2009; Matin and Khan, 2016)

3. Velocity and induced magnetic field

The momentum and induced magnetic field equations are obtained from the Navier-Stokes equations and induction equation respectively as:

$$\rho_f \left( \frac{\partial \vec{v}}{\partial t} + (\vec{v} \cdot \nabla) \vec{v} \right) = -\nabla p + \mu \nabla^2 \vec{v} + \rho_e E_x + \mu_e (\nabla \times \vec{H}) \times \vec{H} \tag{4}$$

$$\frac{\partial \vec{H}}{\partial t} = \nabla \times (\vec{v} \times \vec{H}) + \frac{1}{\sigma \mu_e} \nabla^2 \vec{H} \tag{5}$$

Considering the steady fully developed flow (\$\vec{v} = u(y)\vec{i} + 0\vec{j} + 0\vec{k}\$) and (\$\vec{H} = H\_x(y)\vec{i} + H\_0\vec{j} + 0\vec{k}\$) in the presence of induced magnetic field, pressure gradient and electrokinetic effect, the governing momentum equation becomes:

$$\mu \frac{d^2 u}{dy^2} + \mu_e H_0 \frac{dH_x}{dy} - \frac{dp}{dx} + \frac{d^2 \psi'}{dy^2} \epsilon E_x = 0 \tag{6}$$

While the induced magnetic field equation is obtained from magnetic induction equation as (Gosh et al., 2010):

$$\frac{1}{\mu_e \sigma} \frac{d^2 H_x}{dy^2} + H_0 \frac{du}{dy} = 0 \tag{7}$$

Using suitable dimensionless parameters, Eqs. (6–7) become:

$$\frac{d^2U}{dY^2} + M^2 \frac{dH}{dY} - \frac{dP}{dX} + G_2\psi = 0 \tag{8}$$

$$\frac{d^2H}{dY^2} + \frac{dU}{dY} = 0 \tag{9}$$

subject to the following dimensionless boundary conditions:

$$U(Y) = 0, \quad A_1 \frac{dH(Y)}{dY} + B_1 H(Y) = 0, \quad \text{at } Y = 0 \tag{10}$$

$$U(Y) = 0, \quad A_2 \frac{dH(Y)}{dY} + B_2 H(Y) = 0, \quad \text{at } Y = 1 \tag{11}$$

where the constant  $s$   $A_1, A_2, B_1$  and  $B_2$  assume value zero or one to indicate the electrical conductivity or electrical non-conductivity of the walls (Jha and Aina, 2016; Jha and Sani, 2013; Gosh et al., 2010). For Case I ( $B_1 = B_2 = 1$  and  $A_1 = A_2 = 0$ ) signifies that the both walls are electrically non-conducting, Case II ( $A_1 = B_2 = 1$  and  $B_1 = A_2 = 0$ ) indicates that the lower wall situated at  $Y = 0$  is electrically conducting while the upper wall situated at  $Y = 1$  is electrically non-conducting, Case III ( $A_1 = B_2 = 0$  and  $B_1 = A_2 = 1$ ) shows that the lower wall situated at  $Y = 0$  is electrically non-conducting while the upper wall situated at  $Y = 1$  is electrically conducting.

Since the flow is fully developed, it is usual to assume constant pressure gradient which is obtained from the fluid conservation:

$$\bar{U} = \int_0^1 U(Y) dY = 1 \tag{12}$$

### 3.1. Energy equation

Due to the constant flux at the walls, the energy equation is obtained in dimensional form as (Mukhopadhyay et al., 2009)

$$u \frac{\partial T}{\partial x} = \alpha \frac{\partial^2 T}{\partial y^2} + \frac{S_E}{\rho C_p} \tag{13}$$

Following (Mukhopadhyay et al., 2009), the energy equation in dimensionless form with the associated boundary conditions are given as:

$$\frac{d^2\theta}{dY^2} = \frac{U}{\bar{U}} \left( \frac{1+q_r}{2} + S_E \right) - S_E \tag{14}$$

$$\frac{d\theta(Y)}{dY} = -1 \text{ at } Y = 0, \text{ and } \frac{d\theta(Y)}{dY} = q_r \text{ at } Y = 1 \tag{15}$$

The following dimensionless parameters are used in this current article, and given as follow:

$$M^2 = \frac{\sigma \mu_e^2 H_0^2 b^2}{\mu}, \quad Y = \frac{y}{b}, \quad X = \frac{x}{b}, \quad U = \frac{u}{u_0}, \quad \theta = \frac{(T - T_{ref})}{q_1 b/k},$$

$$P = \frac{p}{\rho u_0^2}, \quad \xi = \frac{\zeta_2}{\zeta_1}, \quad \psi = \frac{zF\psi'}{RT}, \quad \kappa = \frac{b}{\lambda_D}, \quad \lambda_D = \left[ \frac{\epsilon RT}{2F^2 Z^2 C_0} \right]^{1/2},$$

$$G_2 = \frac{2F^2 Z^2 C_0 b^2}{\epsilon RT}, \quad H = \frac{H_x}{\sigma \mu_e b H_0 u_0} \tag{16}$$

It should be mentioned that in the absence of the magnetic field ( $M = 0$ ), all of the flow and heat transfer mathematical model reported above are consistent with those reported earlier by Mukhopadhyay et al. (2009).

### 3.2. Exact solution for the models

The electric potential, velocity profile, induced magnetic field, pressure gradient and temperature distributions of Eqs. (2, 8, 9, 12, 14) are solved with their corresponding boundary conditions respectively to obtain the following exact solutions:

$$\psi(Y) = \frac{[\xi \sinh(\kappa Y) + \sinh\{\kappa(1 - Y)\}]}{\sinh(\kappa)} \tag{17}$$

$$U(Y) = C_3 \cosh(MY) + C_4 \sinh(MY) - \frac{1}{M^2} \frac{dP}{dX} + \frac{G_2[\xi \sinh(\kappa Y) + \sinh\{\kappa(1 - Y)\}]}{(M^2 - \kappa^2) \sinh(\kappa)} \tag{18}$$

$$H(Y) = \frac{Y}{M^2} \frac{dP}{dX} - \frac{\{C_3 \cosh(MY) + C_4 \sinh(MY)\}}{M} - \frac{G_2[\xi \cosh(\kappa Y) - \cosh\{\kappa(1 - Y)\}]}{\kappa(M^2 - \kappa^2) \sinh(\kappa)} + C_5 Y + C_6 \tag{19}$$

$$\frac{dP}{dX} = \frac{D_5 M + D_2 \sinh(M) + D_4(\cosh(M) - 1)}{D_1(M - \sinh(M)) + D_3(1 - \cosh(M))} \tag{20}$$

$$\theta(Y) = \frac{A}{\bar{U}} \left[ \frac{\{C_3 \cosh(MY) + C_4 \sinh(MY)\}}{M^2} - \frac{Y^2}{2M^2} \frac{dP}{dX} + \frac{G_2[\xi \sinh(\kappa Y) + \sinh\{\kappa(1 - Y)\}]}{\kappa^2(M^2 - \kappa^2) \sinh(\kappa)} \right] - \frac{S_E Y^2}{2} + C_7 Y + C_8 \tag{21}$$

$$A = \left( \frac{1+q_r}{2} + S_E \right)$$

The dimensionless skin-friction on both walls are obtained from Eq. (18) and given by:

$$\tau_0 = \left. \frac{dU}{dY} \right|_{Y=0} = C_4 M + \frac{G_2 \kappa [\xi - \cosh(\kappa)]}{(M^2 - \kappa^2) \sinh(\kappa)} \tag{22}$$

$$\tau_1 = - \left. \frac{dU}{dY} \right|_{Y=1} = -M \{C_3 \cosh(M) + C_4 \sinh(M)\} - \frac{G_2 \kappa [\xi \cosh(\kappa) - 1]}{(M^2 - \kappa^2) \sinh(\kappa)} \tag{23}$$

Two important parameters for flow formation with induced magnetics field are induced current density ( $J_\theta$ ) and induced flux density ( $J$ ) which are respectively obtained as:

$$J_\theta = - \frac{dH}{dY} = U(Y) - C_5 \tag{24}$$

$$J = \int_0^1 J_\theta dY = 1 - C_5 \tag{25}$$

Another significant quantity in fluid and thermodynamics is the heat transfer coefficient. The heat transfer between the heated plats and the electrically conducting fluid is represented by Nusselt number and obtained as:

$$Nu_0 = \left. \frac{d\theta}{dY} \right|_{Y=0}, \quad Nu_1 = - \left. \frac{d\theta}{dY} \right|_{Y=1} \tag{26}$$

where  $\theta_m$  is the bulk temperature defined as:

$$\theta_m = \frac{\int_0^1 U(Y)\theta(Y)dY}{\int_0^1 U(Y)dY} = \sum_{i=1}^{24} E_i \tag{27}$$

where  $C_i$ 's,  $D_i$ 's and  $E_i$ 's are constants defined in appendix

**4. Results and discussion**

This article investigate the combined role of transversely applied magnetic field and electrokinetic effect on pressure driven flow in a parallel plates channel with induced magnetic field.

**4.1. Special cases**

From the solutions obtained from Eqs. (18) – (23), a discontinuity point is observed when the Hartmann number ( $M$ ) is equal to the Debye-Hückel parameter ( $\kappa$ ). These quantities are possible to have the same magnitude in real life. Hence in such scenario, the exact solutions obtained in Eqs. (18) – (23) become invalid. To remove this discontinuity, we substitute  $M = \kappa$  in the dimensionless Eqs. (8) – (15) and resolve. Although a degeneracy occur and is removed by using suitable complementary solution for the non-homogeneous part. On solving, the following expressions are obtained for velocity, pressure gradient and induced magnetic field:

$$U_s(Y) = C_9 \cosh(\kappa Y) + C_{10} \sinh(\kappa Y) - \frac{1}{\kappa^2} \frac{dP}{dX} - \frac{G_2 Y}{2\kappa} [C_1 \sinh(\kappa Y) + C_2 \cosh(\kappa Y)] \tag{28}$$

$$\frac{dP}{dX_s} = \frac{(2\kappa^2 - 2\kappa^2 D_{13})\kappa \sinh(\kappa) - G_2 [C_2 \cosh(\kappa) + C_1 \sinh(\kappa)] (\cosh(\kappa) - 1) \kappa \sinh(\kappa)}{2 \{ \sinh(\kappa) (\sinh(\kappa) - \kappa) - (1 - \cosh(\kappa))^2 \}} \tag{29}$$

$$H_s(Y) = \frac{Y}{\kappa^2} \frac{dP}{dX} - \frac{1}{\kappa} [C_9 \sinh(\kappa Y) + C_{10} \cosh(\kappa Y)] + \frac{G_2}{2\kappa^3} [C_1 \{ \kappa^2 \cosh(\kappa Y) - \sinh(\kappa Y) \} + C_2 \{ \kappa^2 \sinh(\kappa Y) - \cosh(\kappa Y) \}] + C_{11} Y + C_{12} \tag{30}$$

From the velocity and induced magnetic field, all other parameters such as temperature, skin-friction, induced flux density and Nusselt number can be obtained when the value of Hartmann number is equal to the Debye-Hückel parameter.

For purely forced convection flow, i.e.  $G_2 = 0$ , from Eqs. (18–23) the velocity, pressure gradient and induced magnetic field reduce to:

$$U_p(Y) = \frac{1}{M^2} \frac{dP}{dX_p} \{ \cosh(MY) + [\text{cosech}(M) - \text{coth}(M)] \sinh(MY) - 1 \} \tag{31}$$

$$H_p(Y) = \frac{Y}{M^2} \frac{dP}{dX_p} - \frac{\{ C_3 \cosh(MY) + C_4 \sinh(MY) \}}{M} + C_{15} Y + C_{16} \tag{32}$$

$$\frac{dP}{dX_p} = \frac{1}{D_1 (\sinh(M) - M) - D_3 (1 - \cosh(M))} \tag{33}$$

$$\theta_p(Y) = \frac{A}{\bar{U}} \frac{1}{M^2} \frac{dP}{dX_p} \left[ \frac{\{ \cosh(MY) + [\text{cosech}(M) - \text{coth}(M)] \sinh(MY) \}}{M^2} - \frac{Y^2}{2} \right] - \frac{S_E Y^2}{2} + C_{17} Y + C_{18} \tag{34}$$

In similar manner, for purely electrokinetic flow, the pressure gradient becomes zero ( $\frac{dP}{dX} = 0$ ) and the fluid is driven by purely asymmetric external voltage gradient and hence the velocity and induced magnetic field becomes:

$$U_e(Y) = \frac{G_2}{(\kappa^2 - M^2)} \{ \cosh(MY) + [\xi \text{cosech}(M) - \text{coth}(M)] \sinh(MY) - \frac{[\xi \sinh(\kappa Y) + \sinh\{\kappa(1 - Y)\}]}{\sinh(\kappa)} \} \tag{35}$$

$$H_e(Y) = \frac{G_2}{(M^2 - \kappa^2)} \{ \cosh(MY) + [\xi \text{cosech}(M) - \text{coth}(M)] \sinh(MY) + \frac{[\xi \cosh(\kappa Y) - \cosh\{\kappa(1 - Y)\}]}{\kappa \sinh(\kappa)} \} + C_{19} Y + C_{20} \tag{36}$$

To have a clearer understanding on flow formation in the channel, graphs and tabular representations are carried out on fluid velocity, induced magnetic field, temperature distribution, skin-friction, induced current density and Nusselt number. Throughout the current research, the Debye-Hückel parameter is taken over the range of  $0 \leq \kappa \leq 30$  to capture various physical situations ranging from small EDL to large EDL,  $0 \leq M \leq 10$  for Hartmann number, the asymmetric external voltage gradient called zeta potential is assumed over  $0 \leq \xi \leq 1$ . Three cases of induced magnetic field are considered; case I, when both walls are non-conducting and has caption (a) in figures, case II, the wall  $Y = 0$  is electrically conducting and has caption (b) in figures while for case III the wall  $Y = 1$  is electrically conducting with caption (c) in figures. It has been stated in literature that mathematical solution cannot be obtained for the case when both walls are simultaneously conducting; this is because of non-existence of solution for this case.

Fig. 2 presents the combined role of Debye-Hückel parameter ( $\kappa$ ) and dimensionless zeta potential ( $\xi$ ) on dimensionless electrostatic potential in the channel. It is found that the EDL potential is higher at the walls due to the supply of external voltage at the walls but decreases with increase in  $\kappa$ . This is due to the fact that increasing  $\kappa$  decreases the Debye-length (EDL size) which in turn decrease EDL potential. A careful look at this figure shows that the electrostatic potential is zero for large value of  $\kappa$  around the centre of the channel; where EDL is minimum.

Fig. 3 depicts the effect of  $\kappa$  and Hartmann number ( $M$ ) on dimensionless fluid velocity in the channel. It is clear from this figure that fluid motion increases with increase in  $\kappa$  at the region

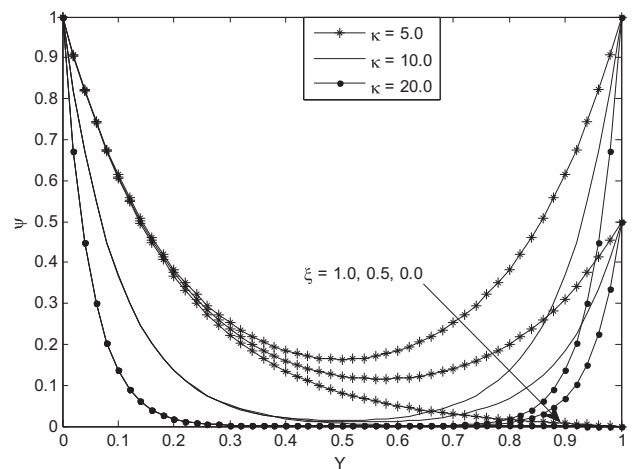


Fig. 2. Electrostatic potential for different values of  $\kappa$  and  $\xi$ .

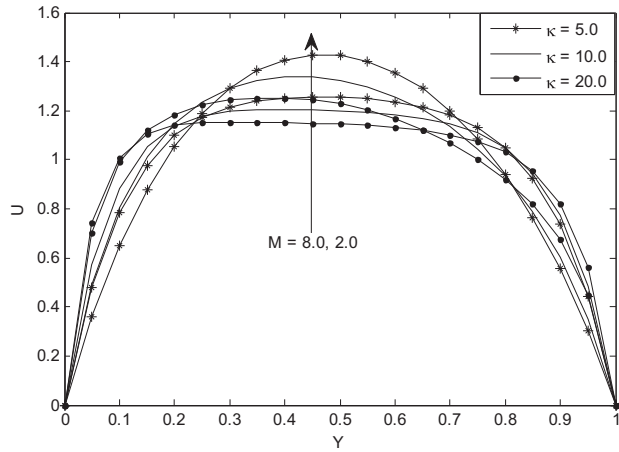


Fig. 3. Velocity profile for different values of  $\kappa$  and  $M$  at  $\zeta = 0.5$ .

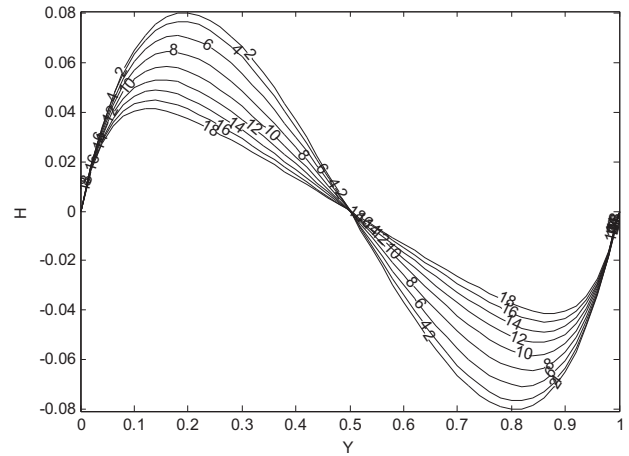


Fig. 5a. Induced magnetic field for different values of  $\kappa$  at  $M = 6.0, \zeta = 1.0$ .

close to the plates, while the reverse trend is noticed at the center of the channel. This can be explained by externally applied voltage gradient at the walls which increases the kinetic energy at the EDL and hence increase fluid velocity at the walls. From the same figure, similar trend is also followed for variation of Hartmann number on fluid velocity in the channel. It is interesting to note that two points of inflexion occur in channel which can be attributed to the constantly applied pressure gradient in the channel.

On the other hand, Fig. 4 shows the impact of zeta potential on dimensionless fluid velocity in the channel. It is obvious that fluid velocity is highest at the center of the channel for purely asymmetric wall voltage gradient ( $\zeta = 0$ ). Contrary to previous figure, a point of connection is observed which can be attributed to the variation of zeta potential whose location in the channel is strictly dependent on  $\kappa$ . It is good to state that at this point, fluid velocity is independent on  $\zeta$ .

Figs. 5a, 5b and 5c portray dimensionless induced magnetic field when both walls are non-conducting, the wall  $Y = 0$  only is conducting and the wall  $Y = 1$  only is conducting respectively for different values of  $\kappa$  at fixed value of  $M$  and  $\zeta$ . Dimensionless induced magnetic field is observe to monotonically decrease with increase in electrokinetic parameter ( $\kappa$ ) in the channel for all cases for  $0 \leq Y \leq 0.5$  while the reverse situation occurs for  $Y > 0.5$ . This can be explained due to the fact that  $\kappa$  is inversely proportion to EDL length and therefore decreases the induced magnetic field. For all cases, a point of intersection is noticed at the center of the

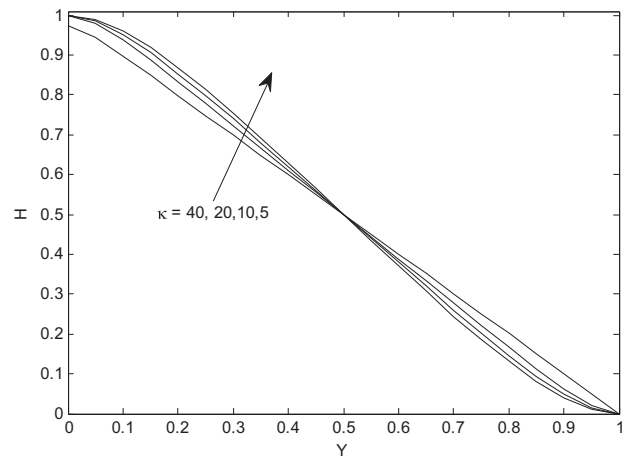


Fig. 5b. Induced magnetic field for different values of  $\kappa$  at  $M = 6.0, \zeta = 1.0$ .

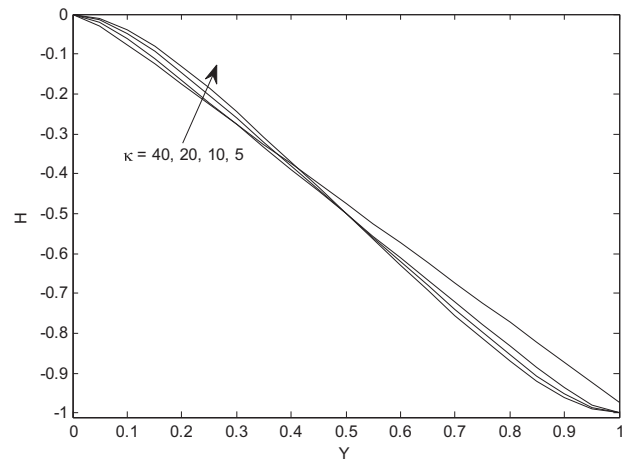


Fig. 5c. Induced magnetic field for different values of  $\kappa$  at  $M = 6.0, \zeta = 1.0$ .

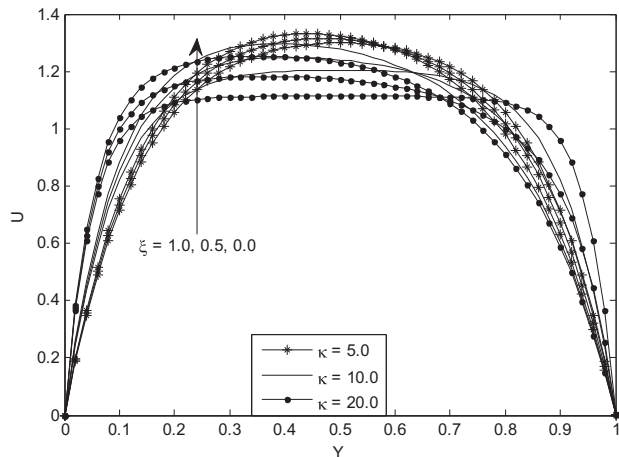


Fig. 4. Velocity profile for different values of  $\kappa$  and  $\zeta$  at  $M = 6.0$ .

channel and at this point, induced magnetic field is independent of electrokinetic parameter ( $\kappa$ ). A critical look at Figs. 5b and 5c suggests that they are converses of each other. Therefore the magnitude of induced magnetic field is the same irrespective of the electrically conducting plates.

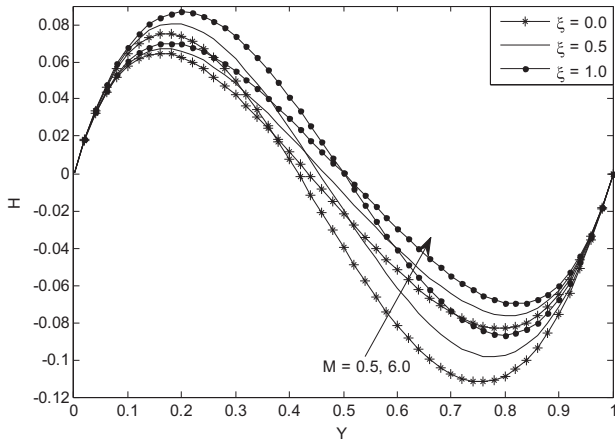


Fig. 6a. Induced magnetic field for different values of  $M$  and  $\xi = 1.0, \alpha\kappa = 5.0$ .

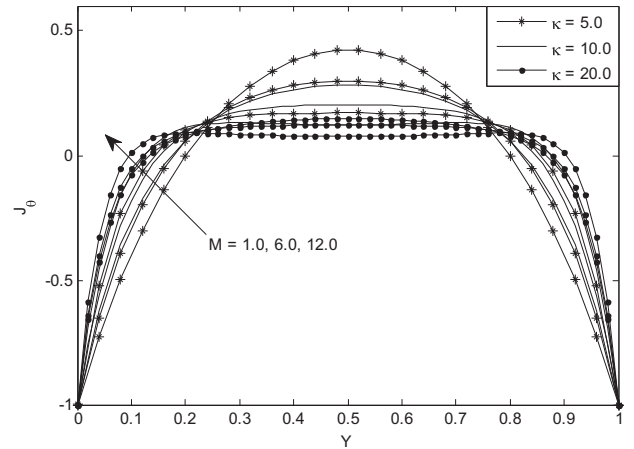


Fig. 7a. Induced current density for different values of  $\kappa$  and  $M = 1.0, 6.0, 12.0$  and  $\xi = 1.0$ .

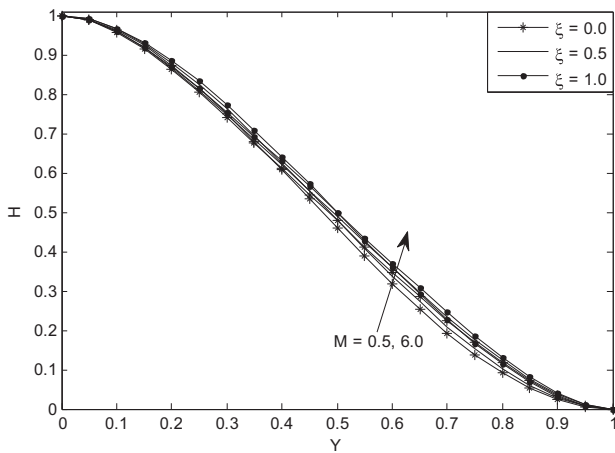


Fig. 6b. Induced magnetic field for different values of  $M$  and  $\xi = 1.0, \alpha\kappa = 5.0$ .

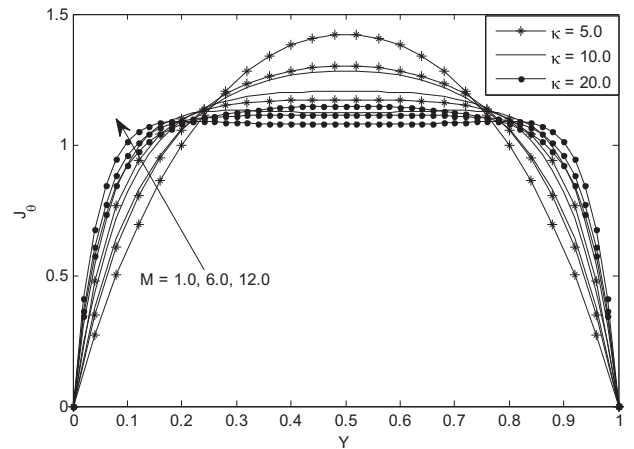


Fig. 7b. Induced current density for different values of  $\kappa$  and  $M = 1.0, 6.0, 12.0$  and  $\xi = 1.0$ .

Figs. 6a and 6b present the combined role of Hartmann number ( $M$ ) and zeta potential ( $\xi$ ) of dimensionless induced magnetic field in the channel for the three cases. For the case when both walls are electrically non-conducting (case I), the generated magnetic field increases with increase in zeta potential and Hartmann number but decreases along the plates for  $Y > 0.2$ .

From Fig. 6b on the other hand, induced magnetic field decreases along the plates monotonically from  $Y = 0$  to  $Y = 1$  but it is evidence to note that the role of magnetic field and zeta potential is to increase dimensionless induced magnetic field. This is attributed to the fact that increase in Hartmann number ( $M$ ) increases the magnetic field strength which in turn enhances induced magnetic field. For brevity, the behaviour of case II and III are similar and hence Fig. 6c is neglected.

The effects of Debye-Hückel parameter ( $\kappa$ ) and Hartmann number ( $M$ ) on dimensionless induced current density is illustrated in Figs. 7a and 7b for case I and II respectively. This figures show that the highest induced current density is obtained at the center of the channel when  $\kappa$  is very small and the case when one of the wall is conducting. It is obvious from both figures that induced current density is enhanced at the walls with increase in  $\kappa$  and  $M$ .

Fig. 8 gives a contour variation of temperature distributions in the channel as a function of  $\kappa$  at fixed value of  $M$  and  $\xi$ . It is observed that dimensionless temperature distribution decreases with increase in  $\kappa$ . This phenomena is expected as continuous increase of  $\kappa$  continually decreases EDL length and hence reduces

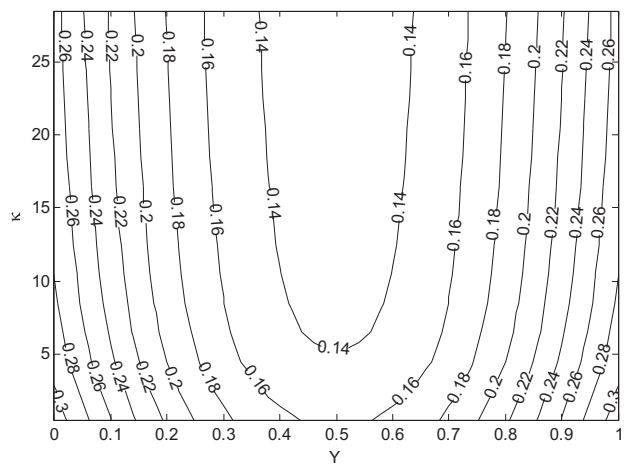


Fig. 8. Temperature distribution ( $\theta - \theta(1)$ ) for different values of  $\kappa$  at  $M = 10, \xi = 1.0, q_r = 1.0, S_E = 0.5$ .

the temperature distribution in the channel. A clearer view of variation of temperature distribution with  $M$  and  $\kappa$  is presented in Fig. 9. This figure shows that the maximum fluid temperature are achieved at the walls where the external voltage gradient is applied. In addition, fluid temperature decreases with increase in

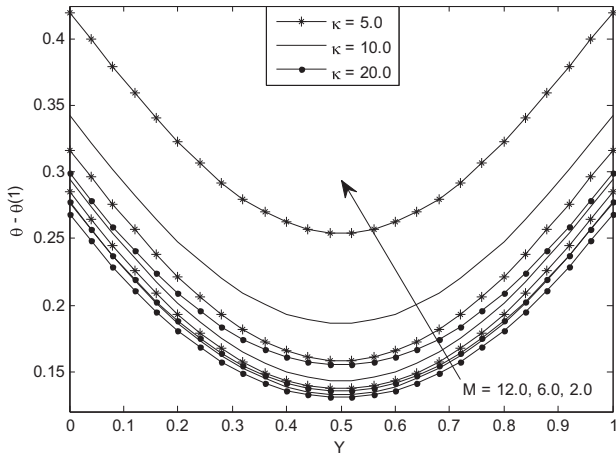


Fig. 9. Temperature distribution for different values of  $\kappa$  and  $Mat\xi = 1.0, q_r = 1.0, S_E = 0.5$ .

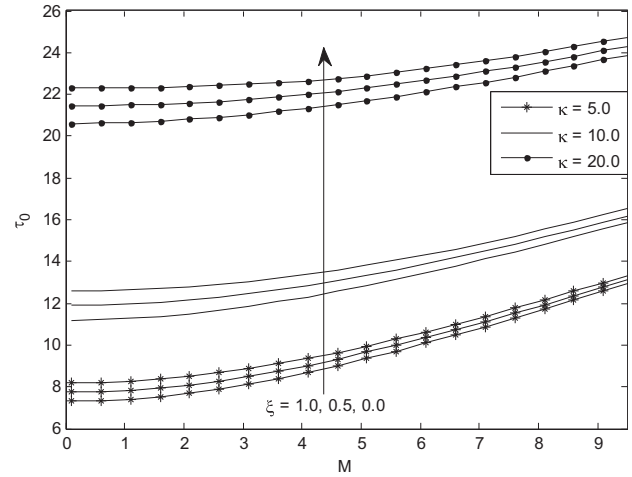


Fig. 11. Skin-friction for different values  $M, \kappa$  and  $\zeta$  at  $Y = 0$ .

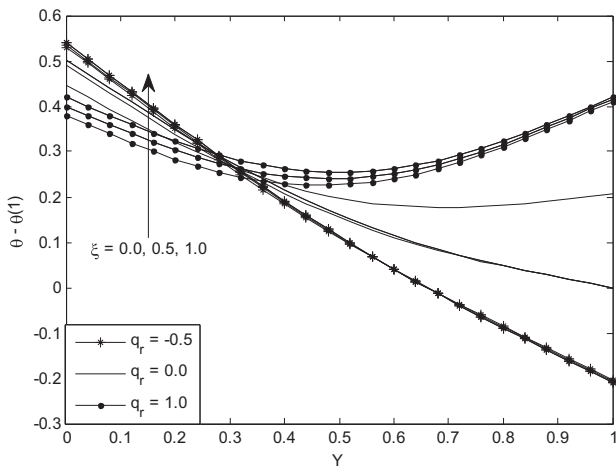


Fig. 10. Temperature distribution for different values  $q_r$  and  $\zeta$  at  $M = 2.0, \kappa = 5.0, S_E = 0.5$ .

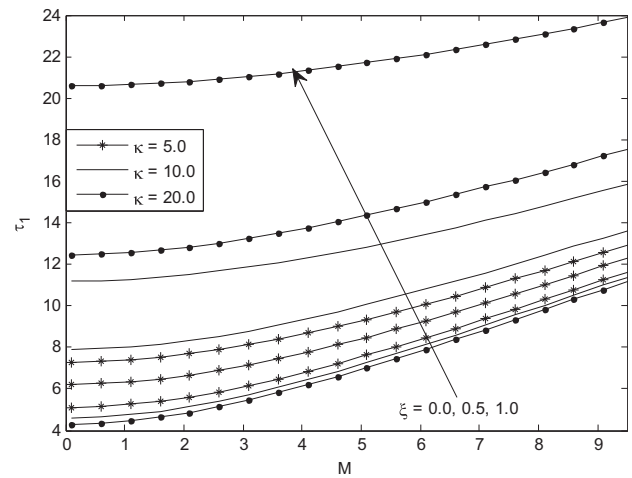


Fig. 12. Skin-friction for different values  $M, \kappa$  and  $\zeta$  at  $Y = 1$ .

$M$  and the lowest temperature distribution is found at the center of the channel.

Fig. 10 displays temperature distributions as a function of zeta potential and wall heat flux at fixed value of  $M$  and  $\kappa$ . It is understandable from this figure that the role of zeta potential is to increase temperature distribution at the region closer to the plate  $Y = 0$  while the converse result is obtained for other region in the channel. Also, fluid emperature decreases with increase in heat flux variation at the region  $Y = 0$  whereas heat flux parameter has little significant at other region for  $q_r = -0.5$ .

One of the important parameter in the study of fluid formation in an enclosed surface is the skin friction. It is defined as the drag force to which fluid hits the walls of the parallel plates. Figs. 11 and 12 reveal variation of skin friction with Debye-Hückel parameter ( $\kappa$ ), zeta potential ( $\zeta$ ) and Hartmann number ( $M$ ) at the lower and upper plates respectively. In both figures, skin-friction is found to increase with increase in  $M$  and  $\kappa$ . This is due to the fact that increasing Hartmann number increases magnetic field strength which in turn increase collision between the plate surfaces and the fluid.

Fig. 11 further shows that the role of zeta potential at this surface is to decrease skin-friction while the reverse trend is observed at the wall  $Y = 1$ .

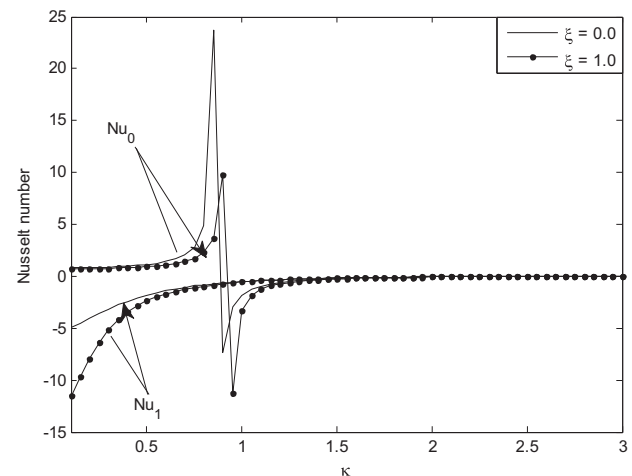


Fig. 13. Nusselt number for different values of  $\kappa$  and  $\zeta$  at  $M = 5.0, q_r = 1.0, S_E = 2.0$ .

Over the years, there have been intense interest in understanding the rate of heat transfer between fluid and surfaces of solid object. This is due to its industrial and domestic applications.

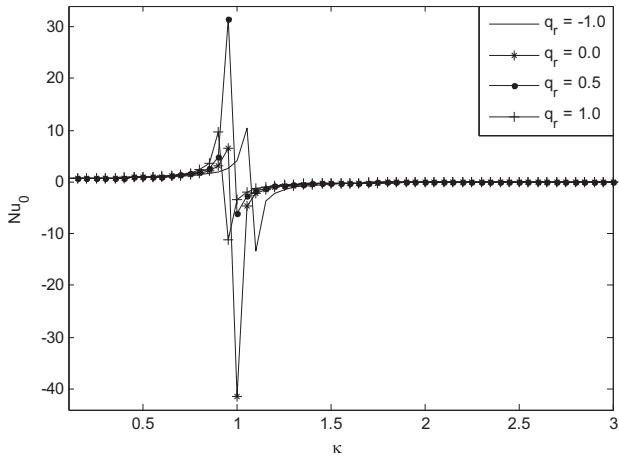


Fig. 14. Nusselt number for different values of  $q_r$  and  $\kappa$  at  $M = 5.0, \zeta = 1.0, S_E = 2.0$ .

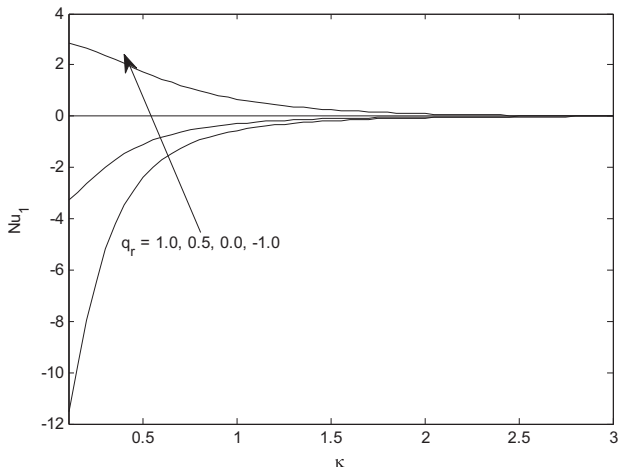


Fig. 15. Nusselt number for different values of  $q_r$  and  $\kappa$  at  $M = 5.0, \zeta = 1.0, S_E = 2.0$ .

Figs. 13, 14 and 15 represent the rate of heat transfer represented by Nusselt number as a function of governing parameters. Fig. 13 depicts the significance of Debye-Hückel parameter ( $\kappa$ ) for symmetric and asymmetric wall zeta potential ( $\zeta$ ) at both surfaces of the channel in the presence of induced magnetic field. For small values of  $\kappa$ , the Nusselt numbers at both walls are very sensitive to both  $\zeta$  and  $\kappa$ . But as  $\kappa \rightarrow \infty$ , The Nusselt numbers at the walls become independent of  $\zeta$  and  $\kappa$  regardless of the surface considered. In addition, the Nusselt number is seen to first increase with  $\kappa$  and then reaches its peak and the start decreasing for small interval of  $\kappa$  but attained a stable value for high values of  $\kappa$  regardless of

the asymmetric in heat flux. This behaviour is observed to happen for any value of zeta potential. As explained in (Mukhopadhyay et al., 2009; Seth and Singh, 2016), this scenario is due to variation of the difference between wall and bulk fluid temperatures.

Similar trend is obtained for variation of Nusselt number with heat flux parameters at the wall  $Y = 0$  in Fig. 14. It has been established from literature (Mukhopadhyay et al., 2009; Maynes and Webb, 2004) that Nusselt number for electrokinetic flow has a non-monotone pattern with negative value due to the fact that for some configurations, where the forward and reverse flows are equivalent, leading to insignificant bulk flow, the smallness of the mean velocity leads to a very high mean temperature, as it is obvious from the definition of bulk mean temperature.

Fig. 15 on the other hand shows a monotone behaviour for variation of Nusselt number with heat flux parameter ( $q_r$ ) in the presence of induced magnetic field at the wall  $Y = 1$ . It is found that Nusselt number decreases with increase  $\kappa$  for the case of symmetric wall heat flux and increases otherwise until a uniform heat transfer coefficient is attained for large value of  $\kappa$ . This behaviour can be attributed to the fact that for large value of  $\kappa$ , a small EDL is setup and the temperature difference between the fluid and the heated wall becomes uniform which in turn results to a zero Nusselt number regardless the value of  $q_r$ .

Table 1 presents numerical computations for induced current flux ( $J$ ) and Nusselt number at the surfaces of the plates. It is obvious that induced current flux is independent on Hartmann number or electrokinetic effect when one of the wall is electrically conducting. In addition, the negative value of Nusselt number can be attributed to the fact that the fluid considered is a heat generating one, this implies the fluid generates more heat than the heat supplied at the walls and has negative heat transfer coefficient. Similar behaviour is found in (Mukhopadhyay et al., 2009). It is good to state that numerical comparison of (Mukhopadhyay et al., 2009) cannot be made with this present work. This is because the pressure gradient was prescribed in their work; which is not a valid assumption for fully developed flow formation. In the current article, the constant pressure gradient is calculated using the conservation of mass in order to present a more scientific and physical situation.

### 5. Conclusion

An exact solution is presented for pressure driven flow formation in a parallel channel plates with electrokinetic effects in the presence of induced magnetic field in this article. Using the Poisson-Boltzmann equation, Debye-Hückel linearization and Navier-Stokes equations, the electric potential, momentum, induced magnetic field and energy equations are derived and solved exactly. Graphical and tabular illustration are presented to see the effects of Debye-Hückel parameter, Hartmann number and zeta potential

Table 1  
Numerical computations for induced current flux ( $J$ ) and Nusselt number at  $\zeta = 0.5, S_E = 2.0, q_r = 1.0$

M	$\kappa$	$Nu_0$	$Nu_1$	J (Induced current flux)		
				$A_1 = A_2 = 0, B_1 = B_2 = 1$ (Case I)	$A_1 = B_2 = 1, A_2 = B_1 = 0$ (Case II)	$A_1 = B_2 = 0, A_2 = B_1 = 1$ (Case III)
0.5	2.0	0.0015	0.0011	-7.1054e-15	1.0000	1.0000
	5.0	-0.0038	-0.0078	0.0000	1.0000	1.0000
	10.0	-3.2196e-07	-3.2197e-07	-4.6185e-14	1.0000	1.0000
4.0	2.0	-0.0471	-0.0440	3.3307e-16	1.0000	1.0000
	5.0	2.8665e-04	2.8678e-04	-4.4409e-16	1.0000	1.0000
	10.0	7.5611e-06	7.5611e-06	-5.6399e-14	1.0000	1.0000
8.0	2.0	-0.0395	-0.0376	6.6613e-16	1.0000	1.0000
	5.0	-1.7924e-04	-1.7920e-04	-1.9096e-14	1.0000	1.0000
	10.0	1.7738e-07	1.7738e-07	-8.4377e-14	1.0000	1.0000

on fluid flow formation. The following are the major conclusions drawn:

1. The role of magnetic field and electrokinetics is to reduce electric potential, velocity, induced magnetic field and fluid temperature.

2. A degeneracy occur when the value of Debye-Hückel parameter equals the Hartmann number.  
3. Skin-friction is enhanced with increase in Debye-Hückel parameter and Hartmann number  
4. Nusselt number in the presence of electrokinetic has a non-monotone pattern

## Appendix

$$\begin{aligned}
 C_1 &= \frac{\xi - \cosh(\kappa)}{\sinh(\kappa)}, C_2 = 1, D_1 = \frac{1}{M^2}, D_2 = \frac{G_2}{(\kappa^2 - M^2)}, D_3 = D_1 [\operatorname{cosech}(M) - \coth(M)], D_4 = D_2 [\xi \operatorname{cosech}(M) - \coth(M)], D_5 = D_2 \left\{ \frac{\cosh(\kappa) - \xi}{\kappa \sinh(\kappa)} - \frac{\sinh(\kappa)}{\kappa} \right\} - 1, \\
 C_3 &= D_1 \frac{dP}{dX} + D_2, C_4 = D_3 \frac{dP}{dX} + D_4, D_6 = A_1 (C_3 - D_1 \frac{dP}{dX} - D_2) + B_1 \left\{ \frac{C_4}{M} - \frac{D_2 (\xi - \cosh(\kappa))}{\kappa \sinh(\kappa)} \right\}, D_7 = (A_2 + B_2), D_8 = A_2 (C_3 \cosh(M) + C_4 \sinh(M) - D_1 \frac{dP}{dX} - D_2 \xi) + \\
 B_2 &\left\{ \frac{C_3 \sinh(M)}{M} + \frac{C_4 \cosh(M)}{M} - D_1 \frac{dP}{dX} - D_2 \left( \frac{\xi - \cosh(\kappa)}{\kappa \sinh(\kappa)} \cosh(\kappa) + \frac{\sinh(\kappa)}{\kappa} \right) \right\}, C_5 = \frac{D_6 B_2 - D_8 B_1}{A_1 B_2 - B_1 D_7}, C_6 = \frac{D_8 A_1 - D_6 D_7}{A_1 B_2 - B_1 D_7}, D_9 = (q_r - 1) - A \left\{ \frac{C_4 (1 + \cosh(M))}{M} + \frac{C_4 \sinh(M)}{M} - \frac{D_2 (\xi - \cosh(\kappa))}{\kappa \sinh(\kappa)} - \right. \\
 D_1 &\frac{dP}{dX} - \frac{D_2}{\kappa} \left( \frac{\xi - \cosh(\kappa)}{\sinh(\kappa)} + \sinh(\kappa) \right) \left. \right\} + S_E, D_{10} = \frac{(1 - \cosh(\kappa))}{\kappa^2 \sinh(\kappa)}, D_{11} = \frac{G_2 (C_2 \cosh(\kappa) + C_1 \sinh(\kappa))}{2\kappa \sinh(\kappa)}, D_{12} = \left[ \frac{\sinh(\kappa)}{\kappa^3} - \frac{1}{\kappa^2} \right], D_{13} = \frac{G_2 C_2}{2\kappa} \left[ \frac{\cosh(\kappa)}{\kappa^2} + \frac{1}{\kappa^2} - \frac{\sinh(\kappa)}{\kappa} \right] - \frac{G_2 C_1}{2\kappa} \left[ \frac{\cosh(\kappa)}{\kappa} - \frac{\sinh(\kappa)}{\kappa^2} \right], \\
 D_{14} &= \frac{\{\cosh(\kappa) - 1\}}{\kappa}, D_{15} = B_1 \left\{ \frac{C_{10}}{\kappa} - \frac{G_2 (\kappa^2 C_1 - C_2)}{2\kappa^3} \right\} - A_1 \left\{ \frac{G_2 (\kappa^2 C_2 - C_1)}{2\kappa^2} - C_9 - \frac{1}{\kappa^2} \frac{dP}{dX} \right\}, D_{16} = A_2 + B_2, D_{17} = A_2 \left[ \frac{1}{\kappa^2} \frac{dP}{dX} + \{C_9 \cosh(\kappa) + C_{10} \sinh(\kappa)\} - \frac{G_2}{2\kappa^2} \{C_1 (\kappa^2 \sinh(\kappa) - \right. \\
 \cosh(\kappa) &+ C_2 (\kappa^2 \cosh(\kappa) - \sinh(\kappa)) \} \right] + B_2 \left[ \frac{\{C_9 \sinh(\kappa) + C_{10} \cosh(\kappa)\}}{\kappa} - \frac{1}{\kappa^2} \frac{dP}{dX} - \frac{G_2}{2\kappa^3} \{C_1 (\kappa^2 \cosh(\kappa) - \sinh(\kappa)) + C_2 (\kappa^2 \sinh(\kappa) - \cosh(\kappa)) \} \right] \\
 C_7 &= \frac{D_9}{2}, C_8 = 0, C_9 = \frac{1}{\kappa^2} \frac{dP}{dX}, C_{10} = D_{10} \frac{dP}{dX} + D_{11}, C_{11} = \frac{D_{17} B_1 - B_2 D_{15}}{B_1 D_{16} - A_1 B_2}, C_{12} = \frac{D_{16} D_{15} - A_1 D_{17}}{B_1 D_{16} - A_1 B_2}, E_1 = \frac{AC_3^2}{M^2} \left( \frac{\sinh(2M)}{4M} + \frac{1}{2} \right), E_2 = \frac{AC_3 C_4}{4M^2} (\cosh(2M) - 1), \\
 E_3 &= -\frac{AC_3}{M^2} \frac{dP}{dX} \sinh(M), E_4 = \frac{AD_2 C_3}{M^2} \left[ \frac{\cosh(\kappa) - \xi}{\sinh(\kappa)} \left\{ \kappa \cosh(\kappa) \cosh(M) - M \sinh(\kappa) \sinh(M) - \frac{\kappa}{(\kappa^2 - M^2)} \right\} - \left\{ \kappa \sinh(\kappa) \cosh(M) - M \cosh(\kappa) \sinh(M) \right\} \right], E_5 = \frac{AC_3 C_4}{4M^2} (\cosh(2M) - 1), \\
 E_6 &= \frac{AC_3^2}{M^2} \left( \frac{\sinh(2M)}{4M} - \frac{1}{2} \right), E_7 = \frac{AC_4}{M^2} \frac{dP}{dX} (1 - \cosh(M)), E_8 = \frac{AD_2 C_4}{M^2} \left[ \frac{\cosh(\kappa) - \xi}{\sinh(\kappa)} \left\{ \frac{\kappa \cosh(\kappa) \sinh(M) - M \sinh(\kappa) \cosh(M)}{(\kappa^2 - M^2)} \right\} - \left\{ \frac{M - M \cosh(\kappa) \cosh(M) - \kappa \sinh(\kappa) \sinh(M)}{(\kappa^2 - M^2)} \right\} \right], \\
 E_9 &= \frac{AC_3}{2M^2} \frac{dP}{dX} \left\{ \frac{2M \cosh(M) - M^2 \sinh(M) - 2 \sinh(M)}{M^2} \right\}, E_{10} = \frac{AC_4}{2M^2} \frac{dP}{dX} \left\{ \frac{2 - 2 \cosh(M) - \cosh(M) + 2M \sinh(M)}{M^2} \right\}, E_{11} = \frac{1}{6M^2} \frac{dP}{dX}, E_{12} = \frac{AD_2}{2M^2 \kappa^3} \frac{dP}{dX} \left[ \frac{\xi - \cosh(\kappa)}{\sinh(\kappa)} \{2 \cosh(\kappa) + \kappa^2 \cosh(\kappa) - \right. \\
 2\kappa \sinh(\kappa) &- 2\} + \{2 \sinh(\kappa) + \kappa^2 \sinh(\kappa) - 2\kappa \cosh(\kappa)\} \right], E_{13} = \frac{AD_2 C_3}{\kappa^2} \left[ \frac{\cosh(\kappa) - \xi}{\sinh(\kappa)} \left\{ \frac{\kappa \cosh(\kappa) \cosh(M) - M \sinh(\kappa) \sinh(M)}{(\kappa^2 - M^2)} - \frac{\kappa}{(\kappa^2 - M^2)} \right\} + \left\{ \frac{\kappa \sinh(\kappa) \cosh(M) - M \cosh(\kappa) \sinh(M)}{M^2 - \kappa^2} \right\} \right], \\
 E_{14} &= \frac{AD_2 C_4}{\kappa^2} \left[ \frac{\cosh(\kappa) - \xi}{\sinh(\kappa)} \left\{ \frac{\kappa \cosh(\kappa) \sinh(M) - M \sinh(\kappa) \cosh(M)}{(\kappa^2 - M^2)} \right\} + \left\{ \frac{M - M \cosh(\kappa) \cosh(M) + \kappa \sinh(\kappa) \sinh(M)}{M^2 - \kappa^2} \right\} \right], E_{15} = \frac{AD_2 D_1}{\kappa^2} \frac{dP}{dX} \left\{ \frac{(\xi - \cosh(\kappa)) (\cosh(\kappa) - 1)}{\kappa \sinh(\kappa)} + \frac{\sinh(\kappa)}{\kappa} \right\}, \\
 E_{16} &= \frac{AD_2^2}{\kappa^2} \left[ \frac{(\xi - \cosh(\kappa))}{\sinh(\kappa)} \left\{ \frac{\sinh(2\kappa)}{4\kappa} - \frac{1}{2} \right\} + \frac{2(\xi - \cosh(\kappa))}{4\kappa \sinh(\kappa)} \{ \cosh(2\kappa) - 1 \} + \left\{ \frac{\sinh(2\kappa)}{4\kappa} - \frac{1}{2} \right\} \right], E_{17} = \frac{S_E C_2}{2} \left\{ \frac{2M \cosh(M) - 2 \sinh(M) - M^2 \sinh(M)}{M^3} \right\}, E_{18} = \\
 -\frac{S_E C_4}{2} &\left\{ \frac{2 - 2 \cosh(M) - M^2 \cosh(M) + 2M \sinh(M)}{M^3} \right\}, E_{19} = \frac{S_E}{6M^2} \frac{dP}{dX}, E_{20} = \frac{S_E D_2}{2\kappa^3} \left[ \frac{(\xi - \cosh(\kappa))}{\sinh(\kappa)} \{2 \cosh(\kappa) + \kappa^2 \cosh(\kappa) - 2\kappa \sinh(\kappa) - 2\} + \{2 \sinh(\kappa) + \right. \\
 \kappa^2 \sinh(\kappa) &- 2\kappa \cosh(\kappa)\} \right], E_{21} = C_3 C_7 \left[ \frac{\sinh(M)}{M} - \frac{\cosh(M)}{M^2} + \frac{1}{M^2} \right], E_{22} = C_4 C_7 \left[ \frac{\cosh(M)}{M} - \frac{\sinh(M)}{M^2} + \frac{1}{M^2} \right], E_{23} = \frac{-C_7}{2M^2} \frac{dP}{dX}, E_{24} = \\
 C_7 D_2 &\left[ \frac{\cosh(\kappa) - \xi}{\sinh(\kappa)} \left\{ \frac{\cosh(\kappa)}{\kappa} - \frac{\sinh(\kappa)}{\kappa^2} \right\} - \left\{ \frac{\sinh(\kappa)}{\kappa} - \frac{\cosh(\kappa)}{\kappa^2} + \frac{1}{\kappa^2} \right\} \right], D_{18} = A_1 (C_{13} - D_1 \frac{dP}{dX}) + B_1 \left\{ \frac{C_{14}}{M} \right\}, D_{20} = A_2 (C_{13} \cosh(M) + C_{14} \sinh(M) - \\
 D_1 &\frac{dP}{dX}) + B_2 \left\{ \frac{C_{13} \sinh(M)}{M} + \frac{C_{14} \cosh(M)}{M} - D_1 \frac{dP}{dX} \right\}, C_{13} = \frac{1}{M^2} \frac{dP}{dX}, C_4 = D_1 [\operatorname{cosech}(M) - \coth(M)] \frac{dP}{dX}, C_{15} = \frac{D_{18} B_2 - D_7 B_1}{A_1 B_2 - B_1 D_7}, C_{16} = \frac{D_{20} A_1 - D_{18} D_7}{A_1 B_2 - B_1 D_7}, \\
 D_{21} &= (q_r - 1) - A \left\{ \frac{C_{14} (1 + \cosh(M))}{M} + \frac{C_{14} \sinh(M)}{M} - D_1 \frac{dP}{dX} \right\} + S_E, C_{17} = \frac{D_{21}}{2}, C_{18} = 0 \\
 D_{22} &= B_1 \left\{ \frac{D_2 [\operatorname{cosech}(M) - \coth(M)]}{M} - \frac{D_2 (\xi - \cosh(\kappa))}{\kappa \sinh(\kappa)} \right\}, D_{23} = A_2 (D_2 \cosh(M) + D_2 [\xi \operatorname{cosech}(M) - \coth(M)] \sinh(M) - D_2 \xi) + B_2 \left\{ \frac{D_2 \sinh(M)}{M} + \right. \\
 \frac{D_2 [\operatorname{cosech}(M) - \coth(M)] \cosh(M)}{M} &- D_2 \left( \frac{\xi - \cosh(\kappa)}{\kappa \sinh(\kappa)} \cosh(\kappa) + \frac{\sinh(\kappa)}{\kappa} \right) \left. \right\}, \\
 C_{19} &= \frac{D_{22} B_2 - D_{23} B_1}{A_1 B_2 - B_1 D_7}, C_{20} = \frac{D_{23} A_1 - D_{22} D_7}{A_1 B_2 - B_1 D_7}
 \end{aligned}$$

## References

Reuss, F.F., 1809. Sur un nouvel effet de l'électricité galvanique. Mémoires de la Société Impériale des Naturalistes de Moscou 2, 327–337.  
 Probst, R.F., 1994. Physicochemical Hydrodynamics: an Introduction. John Wiley & Sons Inc, New York.  
 Helmholtz, H., 1879. Studien über elektrische Grenzschichten. Ann. Phys. 243, 337–382. <https://doi.org/10.1002/andp.18792430702>.  
 Patankar, N.A., Hu, H.H., 1998. Numerical Simulation of Electroosmotic Flow. Anal. Chem. 70, 1870–1881.  
 Ren, L., Li, D., 2001. Electroosmotic flow in heterogeneous microchannels. J. Colloid Interface Sci. 243, 255–261.  
 Yang, C., Li, D., 1998. Analysis of Electrokinetic Effects on the Liquid Flow in Rectangular Microchannels. J. Colloids Surfaces 143, 339–353. 22.  
 Debye, P., Hückel, E., 1923. The theory of electrolytes. I. Lowering of freezing point and related phenomena. Physikalische Zeitschrift 24, 185–206.  
 Zade, A.Q., Manzari, M.T., Hannani, S.K., 2007. An analytical solution for thermally fully developed combined pressure-electroosmotically driven flow in microchannels. Int. J. Heat Mass Transfer 50, 1087–1096.  
 Mukhopadhyay, A., Banerjee, S., Gupta, C., 2009. Fully developed hydrodynamic and thermal transport in combined pressure and electrokinetically driven flow in a

microchannel with asymmetric boundary conditions. Int. J. Heat Mass Transf. 52, 2145–2154.  
 Soong, C.Y., Wang, S.H., 2003. Theoretical analysis of electrokinetic flow and heat transfer in a microchannel under asymmetric boundary conditions. J. Colloid Interface Sci. 265, 202–213.  
 Matin, M.H., Khan, W.A., 2016. Electrokinetic effects on pressure driven flow of viscoelastic fluids in nanofluidic channels with Navier slip condition. J. Mol. Liq. 215, 472–480.  
 Rossow, V.J., 1957. Flow of electrically conducting fluids over a flat plate in the presence of a transverse magnetic field. Report 1358 National Advisory Committee for Aeronautics.  
 Ibrahim, D.K., 1967. Effects of induced magnetic field on inviscid magnetohydrodynamics channel flow, Retrospective Thesis and Dissertations paper 3925.  
 Jha, B.K., Oni, M.O., 2017. Impact of mode of application of magnetic field on rate of heat transfer of rarefied gas flow in a microtube. Alexandria Engr. J. <https://doi.org/10.1016/j.aej.2017.03.029>.  
 Jha, B.K., Aina, B., Isa, S., 2015. Fully developed MHD natural convection flow in a vertical microchannel: an exact solution. J. King Saud Univ.-Sci. 27, 253–259.  
 Jha, B.K., Aina, B., 2016. Role of induced magnetic field on MHD natural convection flow in a vertical microchannel formed by two electrically non-conducting

- infinite vertical parallel plates. Alexandria Engr. J. <https://doi.org/10.1016/j.aej.2016.06.030>.
- Jha, B.K., Sani, I., 2013. Computational treatment of MHD of transient natural convection flow in a vertical channel due to symmetric heating in the presence of induced magnetic field. *J. Phys. Soc. Jpn.* **82**, 084401.
- Gosh, S.K., Beg, O.A., Zueco, J., 2010. Hydromagnetic free convection flow with induced magnetic field effects. *Meccanica* **14**, 175–185.
- Das, S., Mitra, S.K., 2012. Magnetohydrodynamics in narrow fluidic channels in presence of spatially non-uniform magnetic fields: framework for combined magnetohydrodynamic and magnetophoretic particle transport. *Microfluid Nanofluid* **13**, 799–807. <https://doi.org/10.1007/s10404-012-1001-z>.
- Ganguly, S. et al., 2015. Thermally developing combined electroosmotic and pressure-driven flow of nanofluids in a microchannel under the effect of magnetic field. *Chem. Eng. Sci.* **126**, 10–21.
- Sarkar, S. et al., 2014. Buoyancy driven convection of nanofluids in an infinitely long channel under the effect of a magnetic field. *Int. J. Heat Mass Transf.* **71**, 328–340.
- Sarkar, S., Ganguly, S., 2018. Fully developed thermal transport in combined pressure and electroosmotically driven flow of nanofluid in a microchannel under the effect of a magnetic field. *Microfluid Nanofluid.* doi:10.1007/s10404-014-1461-4.
- Sarkar, S., Ganguly, S., Dutta, P., 2017. Electrokinetically induced thermofluidic transport of power-law fluids under the influence of superimposed magnetic field. *Chem. Eng. Sci.* <https://doi.org/10.1016/j.ces.2017.05.053>.
- Sarkar, S., Ganguly, S., Chakraborty, S., 2017. Influence of combined electromagnetohydrodynamics on microchannel flow with electrokinetic effect and interfacial slip. *Microfluid Nanofluid* **21**, 56. <https://doi.org/10.1007/s10404-017-1894-7>.
- Sarkar, S. et al., 2017. Thermofluidic characteristics of combined electroosmotic and pressure driven flows in narrow confinements in presence of spatially non-uniform magnetic field. *Int. J. Heat Mass Transf.* **104**, 1325–1340.
- Seth, G.S., Singh, J.K., 2016. Mixed convection hydromagnetic flow in a rotating channel with Hall and wall conductance effects. *Appl. Math. Modelling* **40**, 2783–2803.
- Maynes, D., Webb, B.W., 2004. The effect of viscous dissipation in thermally fully developed electro-osmotic heat transfer in microchannels. *Int. J. Heat Mass Transf.* **47**, 987–999.